DTIC FILE COPY

AD-A218 896

DTIC ELECTE MAR 05 1990 D CS

REPORT DOCUMENTATION PAGE

1b RESTRICTIVE MARKINGS: NONE

3 DISTRIBUTION / AVAILABILITY OF REPORT: Approved for public release. Distribution unlimited. (2)

2b DECLASSIFICATION / DOWNGRADING SCHEDULE:

4 PERFORMING ORGANIZATION REPORT NUMBER(S): Technical Report No. 22

5 MONITORING ORGANIZATION REPORT NUMBER(S):

6a NAME OF PERFORMING ORGANIZATION: Massachusetts Institute of Technology

6b OFFICE SYMBOL (If applicable):

7a NAME OF MONITORING ORGANIZATION: ONR

6c ADDRESS (City, State, and ZIP Code): 77 Massachusetts Avenue, Room 1-306, Cambridge, MA 02139

7b ADDRESS (City, State, and ZIP Code): 800 North Quincy Street, Arlington, VA 22217

8a NAME OF FUNDING / SPONSORING ORGANIZATION: DARPA

8b OFFICE SYMBOL (If applicable):

9 PROCUREMENT INSTRUMENT IDENTIFICATION NUMBER: N00014-86-K-0768

8c ADDRESS (City, State, and ZIP Code): 1400 Wilson Boulevard, Arlington, VA 22209

10 SOURCE OF FUNDING NUMBERS

PROGRAM ELEMENT NO.	PROJECT NO.	TASK NO.	WORK UNIT ACCESSION NO.
R & T Code	A 400005		

11 TITLE (Include Security Classification): INVESTIGATION OF ATOMISTIC SIMULATION OF STRUCTURAL AND DYNAMIC DIFFERENCES IN GLASSY AND LIQUID STATES OF ATACTIC POLY(PROPYLENE)

12 PERSONAL AUTHOR(S): Mark F. Sylvester; Sidney Yip; and Ali S. Argon

13a TYPE OF REPORT	13b TIME COVERED	14 DATE OF REPORT (Year, Month, Day)	15 PAGE COUNT
Interim Technical	FROM 1988 TO 1989	1989 December 1	34

16 SUPPLEMENTARY NOTATION: Chapter in "Computer Simulation of Polymers," edited by R.J. Roe, American Chemical Society, Washington, D.C.

17 COSATI CODES		
FIELD	GROUP	SUB-GROUP

18 SUBJECT TERMS (Continue on reverse if necessary and identify by block number): Computer simulation; structural relaxations in glassy polymers; glass transition

19 ABSTRACT (Continue on reverse if necessary and identify by block number)

Atomistic simulation techniques, in conjunction with experimental and theoretical approaches, have proven themselves to be useful tools for the study of materials. Recent years have seen the first application of a variety of simulation methods to investigating the phenomena occurring in bulk polymers [1-5]. Among these, possibly the most important and challenging is the glass transition. Despite its significance, the glass transition is still poorly characterized except in a phenomenological manner.

For instance, comprehension of how the structure of a polymer glass differs from that of the liquid is limited to the somewhat vaguely defined concept of "free volume"[6-7]. It is not known how the volume associated with atoms might be distributed within the polymer or how changes in the distribution are related to the property changes seen at the glass transition. In addition, what other structural changes occur on passing between the liquid and glass states are not known.

Likewise, the change in chain dynamics which occurs on passage through the glass

(over)

20 DISTRIBUTION / AVAILABILITY OF ABSTRACT: ☒ UNCLASSIFIED/UNLIMITED ☐ SAME AS RPT ☐ DTIC USERS

21 ABSTRACT SECURITY CLASSIFICATION: Unclassified

22a NAME OF RESPONSIBLE INDIVIDUAL: Dr. Kenneth Wynne

22b TELEPHONE (Include Area Code): (202)696-4100

22c OFFICE SYMBOL:

DD FORM 1473, 84 MAR — 83 APR edition may be used until exhausted. All other editions are obsolete

SECURITY CLASSIFICATION OF THIS PAGE

19. ABSTRACT (continued)

transition is not understood beyond the idea that a shift from long range chain motion to local, correlated motion must take place. The nature of these motions or the definition of the terms "long range" and "local" remains to be established.

These questions involve the local atomic level structure and motion of individual or small groups of atoms. Available experimental and theoretical methods are not well suited to investigate these details. Therefore, simulation is the only way to obtain physical insight into these problems at the present time. Reported here are initial results obtained from a serie of such computer simulations carried out on a simple vinyl polymer, atactic poly(propylene).

Investigation by Atomistic Simulation of Structural and Dynamic Differences in the Glassy and Liquid States of Atactic Poly(propylene)

M. F. Sylvester, S. Yip, and A. S. Argon
Massachusetts Institute of Technology
Cambridge, Massachusetts 02139

Introduction

Atomistic simulation techniques, in conjunction with experimental and theoretical approaches, have proven themselves to be useful tools for the study of materials. Recent years have seen the first application of a variety of simulation methods to investigating the phenomena occurring in bulk polymers [1-5]. Among these, possibly the most important and challenging is the glass transition. Despite its significance, the glass transition is still poorly characterized except in a phenomenological manner.

For instance, comprehension of how the structure of a polymer glass differs from that of the liquid is limited to the somewhat vaguely defined concept of "free volume" [6, 7]. It is not known how the volume associated with atoms might be distributed within the polymer or how changes in the distribution are related to the property changes seen at the glass transition. In addition, what other structural changes occur on passing between the liquid and glass states are not known.

Likewise, the change in chain dynamics which occurs on passage through the glass transition is not understood beyond the idea that a shift from long range chain motion to local, correlated motion must take place. The nature of these

motions or the definition of the terms "long range" and "local" remains to be established.

These questions involve the local atomic level structure and motion of individual or small groups of atoms. Available experimental and theoretical methods are not well suited to investigate these details. Therefore, simulation is the only way to obtain physical insight into these problems at the present time. Reported here are initial results obtained from a series of such computer simulations carried out on a simple vinyl polymer, atactic poly(propylene).

Simulation Methodology

Among simulation techniques, molecular dynamics (MD) is most appropriate for directly probing a time dependent phenomenon such as the glass transition. In MD, the system of atoms or molecules is represented by point masses obeying the laws of classical mechanics. The "atoms" interact through semi-empirical inter-atomic potentials that mimic the true quantum mechanical nature of the system. The time evolution of this system is followed and properties of interest are calculated using the precepts of classical statistical mechanics.

The equations of motion governing the phase space trajectory of the simulated atoms are found by the solution of Lagrange's equation, once a system Lagrangian, $\mathcal{L}$, is defined. The choice of $\mathcal{L}$ establishes the character of the statistical mechanical ensemble being simulated. For comparison with experimental results, it is most desirable to simulate the isothermal - isobaric ensemble. This can be accomplished by using the extended system methods of Nosé and Hoover [8, 9] for the isothermal ensemble and Andersen [10], as modified by

Nosé and Klein [11], for the isobaric ensemble. The combined ensemble Lagrangian is:

$$\mathcal{L} = \frac{1}{2}\sum_{i=1}^{N} m_i \xi^2 L^2 \mathbf{s}_i^T \mathbf{g}^T \mathbf{g}\, \mathbf{s}_i - \sum_{i=1}^{N}\sum_{j>i} \phi_{ij}(r_i, r_j) - \sum_{i=1}^{N}\sum_{j>i}\sum_{k>j} \phi_{ijk}(r_i, r_j, r_k) -$$
$$\sum_{i=1}^{N}\sum_{j>i}\sum_{k>j}\sum_{l>k} \phi_{ijkl}(r_i, r_j, r_k, r_l) + \frac{1}{2}W\dot{L}^2 - pL^3|\mathbf{g}| + \frac{1}{2}Q\dot{\xi}^2 - NkT\ln(\xi)$$

where $\mathbf{s}_i$ is the position of the i^{th} particle within the simulation cell, m_i its mass, $\mathbf{g}$ is a 3 x 3 constant matrix describing the shape of the simulation cell (Figure 1a), L is the added degree of freedom (DOF) which controls the dilation/compression of the simulation cell, the ϕ's are the particle potential energies which are a function of the particle positions ($r_i = L\mathbf{g}\mathbf{s}_i$), W the "mass" of the cell DOF, p the externally applied hydrostatic pressure, ξ the thermostating DOF, Q the "mass" of the thermostat DOF, T the desired system temperature, k the Boltzman constant, and N the number of particles in the simulation.

The first term in the Lagrangian represents the kinetic energy of the particles ("atoms") in the simulation cell while the next three the contribution to the particle potential energy arising from two, three, and four body interactions, respectively. The fifth term is the kinetic energy of the simulation cell degree of freedom, and the sixth the potential energy due to an alteration of the cell volume. The last two terms are the kinetic and potential energy contributions from the thermostat degree of freedom.

The identity of the material being simulated is set by the choice of the particle masses, and their interaction potential energy functions, ϕ. For the case of atactic poly(propylene), three particles are used to build the simulated polymer,

following the work of Theodorou and Suter [1]. Explicit atoms are used for the backbone carbon (12 amu) and pendant hydrogens (1.007 amu). However, the three hydrogens and carbon of the pendant methyl groups are represented by a single particle of mass 15.021 amu. Figure 1b shows a schematic picture of a short segment of such an atactic poly(propylene) chain. This "unified atom" approximation should not have a significant effect on the behavior of the model as the internal motions of the methyl group are thought not to effect the properties of the polymer except at very low temperatures. Computationally, it reduces the number of degrees of freedom in the simulated system considerably.

In order to simulate the polymer bulk while still keeping the computational problem to a manageable size, the technique first utilized by Theodorou and Suter has been adopted. The bulk is imitated by a single polymer chain packed in the simulation cell through the use of periodic boundary conditions and image chains. Figure 2 shows one such chain in the simulation cell and unpacked. As can be seen, whenever the chain exits through one wall of the cell, an image chain enters through the opposite wall.

The use of this approximation certainly affects phenomena which occur over long times and distances (e.g. chain diffusion). It should not affect the more local behavior we are interested in, so long as the persistence length of the chain is small compared to the contour length of the chain and smaller than the simulation cell.

Potential energy functions are used to describe the interactions of the particles in the simulation. For a relatively simple non-polar polymer such as

poly(propylene), potentials are required only to describe covalent bonds, intrinsic torsional barriers, and dispersion forces. While complex potentials have been developed for these [12], simpler forms are preferable for the polymer model to minimize the computational burden.

The well known Lennard-Jones 6-12 function is used for the dispersion forces,

$$\phi_{ij}(r_i, r_j) = 4\varepsilon_{ij}\left(\left(\frac{\sigma_{ij}}{|r_{ij}|}\right)^{12} - \left(\frac{\sigma_{ij}}{|r_{ij}|}\right)^{6}\right)$$

where $|r_{ij}|$ is the distance between particles i and j and ε_{ij} and σ_{ij} are constants for each pair of particle types. Following the usual procedure, the potential function is truncated for all $|r_{ij}| > 2.33\sigma_{ij}$. In addition, a quintic spline in the range $1.45\sigma_{ij} > |r_{ij}| > 2.33\sigma_{ij}$ was used to force the potential and its derivatives to go smoothly to zero at the cutoff.

The covalent structure of the model polymer is formed through the use of two simple harmonic potentials, one in the covalent bond length and the other in the valence angle,

$$\phi_{ij}(r_i, r_j) = C_{ij}^{bl}\left(|r_{ij}| - r_{ij}^{o}\right)^2$$

$$\phi_{ijk}(r_i, r_j, r_k) = C_{ijk}^{\theta}\left(\theta_{ijk} - \theta_{ijk}^{o}\right)^2$$

where C_{ij}^{bl} and r_{ij}^{o} are constants for each type of covalent bond, C_{ijk}^{θ} and θ_{ijk}^{o} are constants for each type of valence angle, $|r_{ij}|$ is again the distance between particles i and j, and θ_{ijk} the angle formed by particles i, j, and k.

Finally, the intrinsic barrier to rotation about backbone carbon-carbon bonds is incorporated using a three-fold cosine function,

$$\phi_{ijkl}(r_i, r_j, r_k, r_l) = \frac{1}{2} C^{\omega}_{ijkl}[\cos(3\omega_{ijkl}) + 1]$$

where C^{ω}_{ijkl} is a constant, and ω_{ijkl} is the torsional angle defined by the four backbone particles i, j, k, and l.

The values used for the parameters in the potential functions are given in Table 1. These values were obtained from several sources. Those for the Lennard-Jones potential and the intrinsic torsional potential were taken from Theodorou and Suter [1]. The values for C^{θ}_{ijk} were taken from the work of Suter and Flory [13] while the θ^{o}_{ijk}'s were found by trial and error such that the average equilibrium valence angles agreed with the fixed values used by Theodorou and Suter. Likewise, the parameters for the bond stretch potential were repeatedly adjusted until the equilibrium bond lengths agreed with the fixed values of Theodorou and Suter and frequencies of the bond stretch vibrations roughly agreed with the known experimental values.

Two final parameters used in the model are W and Q, the "masses" of the degrees of freedom which control the temperature and pressure. Their value controls the inertia of these DOF's and hence the response time of the system to changes in T or p. On the other hand, average or equilibrium, properties do not depend on what W and Q are. Values for W and Q (Table 1) were chosen that were large enough to provide the model with numerical stability and small enough to allow the response of the model to be controlled by the response of the simulated polymer chain rather than the additional DOF's.

Preparation of the polymer structures used as input to the MD simulation was carried out using the technique developed by Theodorou and Suter. [1] This process consists of generation of an initial guess for the chain configuration using a Rotational Isomeric States/Monte Carlo scheme followed by an energy minimization to relax the structure to mechanical equilibrium.

These initial structures have fixed covalent bond lengths and valence angles. Furthermore, they are completely static, equivalent to a structure at 0°K. Temperature enters the procedure only in setting the system density and statistical weights used in the RIS generation. In order to use these structures in the molecular dynamics simulation, it is necessary to equilibrate them, introducing thermal motion and allowing the bond lengths and valence angles to take on a distribution of values about the desired ones.

To do this, a series of start-up simulations were used. Based on trials with the model, it was found that an effective schedule is to, first, give the particles in the system a random Maxwellian velocity distribution appropriate for the desired temperature. Second, run the model in a microcanonical ensemble (constant total energy, constant volume) for five picoseconds of simulated time with occasional rescaling of the particle velocities to add kinetic energy to the system. This allows the distributions on bond lengths and angles to form and some partitioning of the kinetic energy. Third, run the simulation for 40 picoseconds in the canonical ensemble (constant temperature, constant volume). This permits continued partitioning of the kinetic energy among the modes available to the system. During this time partial relaxation of the system towards a new mechanical equilibrium consistent with the additional degrees of freedom added to

the system by both the particle momenta and the release of the fixed bond lengths and angles also occurs. Finally, run the simulation for a further 40 picoseconds in the isobaric-isothermal ensemble to allow the volume to relax to an equilibrium value for the system. At the end of this process the system is in full mechanical equilibrium as indicated by an essentially zero internal pressure (< ~±5 atms) and the kinetic energy appears to be partitioned among the modes available to the system.

To carry out the study of how the structure and dynamics of the polymer glass and liquid differ, simulations were carried out at six temperatures -- 393, 343, 293, 233, 213, and 173°K. Three are above the experimental T_g (253°K) and three below. At each temperature, three initial structures of degree of polymerization 76 (455 total atoms) were created at the experimental density for each temperature. These initial structures were equilibrated as described above. The phase space trajectories of each structure were recorded over the last 20 picoseconds of the equilibration process and used for analysis.

The use of the three initial structures for each temperature was necessitated by the sluggishness of the simulation. While ergodic, the time required to allow a single structure to probe a wide volume of phase space is extremely long. Therefore, it was far more efficient to use the multiple initial structures to start in widely separated regions of phase space.

Likewise, it was more efficient to prepare statically equilibrated structures at each temperature than, for instance, to prepare the low temperature simulations by quenching from higher temperatures. Using present day computers, molecular dynamics is capable of studying only phenomena that occur on a time

scale of under a nanosecond. The time required for a polymer system to fully respond to a large temperature change is many orders of magnitude greater than this.

To investigate the structure of the simulated polymer use was made of the technique of Voronoi tessellation of space. [14, 15] Voronoi tessellation is a method of sub-dividing a volume with space-filling convex polyhedra around a given set of reference points within the volume. In this instance, the reference points are the locations of the atoms in the simulation. Especially useful for the purposes of this work is the property of Voronoi polyhedra that every point within a polyhedron is closer to the enclosed reference point than to any other reference point. Therefore, Voronoi tessellation allows the unambiguous apportionment of the volume of the system among each of the atoms in the simulation.

The recorded positions of the atoms were used to tessellate the simulation volume at regular time intervals over the final 20 ps of each simulation. Since it would be expected that the atoms making up each achiral CH_2 or chiral CHR group would make most significant motions as a unit, it was more appropriate to look at the volume associated with each group, or "chain segment", rather than each atom separately. Consequently, the polyhedra for the three atoms in each chain segment were joined together into a "super-polyhedron". For each simulation, the volume distribution of the super-polyhedra was calculated as were the distributions of volumes for neighbors of particular polyhedra.

Results and Discussion

It is desirable to compare the output from a computer simulation to experimental results whenever possible. Experimental data for atactic poly(propylene) is skimpy, but Figures 3 through 5 present three examples of such comparisons.

Figure 3 shows the calculated and experimental [16] X-ray structure factor for atactic poly(propylene) in the low Q region. The agreement in peak positions and relative heights is excellent and indicates the model polymer reproduces the intermolecular structure of the actual material. In the high Q region (not shown) agreement was less good -- particularly in peak heights. The intensity variation in the high Q area mostly reflects intramolecular spatial correlations between atoms. Hence, the lack of agreement in this region is thought to be primarily due to the loss of the contributions from the hydrogens and carbons in the pendant methyl groups which are ignored in the model polymer.

The calculated generalized vibrational frequency spectrum at 233°K and 393°K is presented in Figure 4. The tickmarks along the abscissa indicate the experimental frequencies of the major optical absorption peaks reported for the polymer. [17] Agreement between the location of these peaks and the major peaks in the calculated vibrational frequency spectrum is acceptable given the approximations associated with the simple model potentials. It may be noted that fine features such as the splitting of the methylene C-H stretching (2800-3100 cm^{-1}) into symmetric and anti-symmetric modes are apparently reproduced by the model.

Extra peaks may be seen in the calculated frequency spectrum, particularly those in the region 1200-1500 cm^{-1}. The generalized frequency spectrum is a

distribution of vibrational modes weighted by the square of the vibrational amplitude. It does not take into account optical selection rules and indicates what vibrational modes are present which could absorb optical energy rather than which ones do. Hence, some discrepancy is expected. In addition, the use of a single particle to represent the methyl groups will result in new vibrational modes not found in the actual polymer and a loss of the stretching, bending and torsional modes internal to the methyl group.

Figure 5 shows the specific volume of the simulated polymer versus temperature. Also shown are the experimental values [18] used as the starting points of the simulations at the same temperatures. It can be seen that the simulation duplicates the experimental values to within 5%. Furthermore, the simulated volume-temperature curve displays the change in slope conventionally taken to signify the glass transition. The transition temperature for the simulation is 277°K in contrast to the experimental value of 253°K. The calculated volumetric expansion coefficients also agree quite well with the measured values.

While the agreement of the experimental and calculated volume expansion curve is quite good, it must be emphasized that the calculated curve was not produced by quenching the simulated polymer system from the liquid state, in contrast to the experimental procedure. As described earlier, the simulations at each temperature were started at the experimentally determined specific volume for that temperature and allowed to evolve to mechanically stable states. The residual time average pressure at these states was quite low, and under ~±5 atms for all simulations.

From these results it can be concluded that the molecular dynamics model is a physically reasonable description of the actual polymer. Further analysis of the structure and dynamics of the simulated polymer is therefore warranted.

Figures 6 and 7 depict the distribution of Voronoi volume associated with all chain segments, achiral (CH_2) chain segments, and chiral (CHR) chain segments at 233°K and 393°K. These distributions are representative of the results for the other temperatures above and below the glass transition. Several things may be noted. First, the chiral groups occupy more volume than the achiral groups. This might be expected since the chiral segments contain a bulky methyl group.

Second, the distribution of segment volumes is found to be quite wide with a pronounced large volume tail, particularly for the chiral groups. A small fraction of segments have far more volume associated with them than their minimum van der Waals volume. Presumably, segments with more than minimum volume represent excess or free volume. The breadth of the distributions implies that the excess volume in the system is not shared evenly among the chain segments, but rather tends to be localized.

Third, some differences can be noted between the distributions above and below the glass transition. There is an overall upwards shift in volume at the higher temperature, as would be expected from Figure 5. In addition, the distributions at 393°K seem broader and flatter than those at 233°K.

A more quantitative characterization of these perceptions is presented in Figures 8 and 9, which display plots of the average volume and the standard deviation of the volume distributions against temperature. The average volume

of the achiral and chiral segments increases uniformly with temperature and a slight difference in the slope of the two curves above and below the glass transition is discernable (Figure 8). As the two curves are essentially parallel, it can be deduced that both chiral and achiral groups contribute equally to the overall volume expansion.

From Figure 9 it appears that there is a slight increase in the breadth of the distribution above the glass transition. The average standard deviation of the achiral segments in the structures above T_g was 23% higher than that of the segments below T_g. For the chiral segments the increase was found to be only 15%. Examination of the distributions revealed that most of the increase was due to an increase in the number of segments with significantly larger than average volume, i.e. an enhancement of the large volume tails of the distributions. There were however still a sizable fraction of chain segments with a surprisingly small volume, even at temperatures well into the liquid region.

Taken together, these facts indicate that the overall volume expansion with increasing temperature does not occur solely by a uniform dilation of the volume associated with all segments. Instead, it takes place, in part, by a process in which the population of chain segments with considerable excess volume is increased. This change appears to occur most noticeably around the glass transition temperature.

Since Figures 6-9 indicate that the segment volume is not distributed homogeneously, an important question is what the nature of the spatial distribution of segment volume might be. Figure 10 and 11 provide information which begins to answer this. Both show, first, the distribution of volume associated with all

polymer chain segments and, second, the distribution of volume associated with all segments which are nearest neighbors to an achiral or chiral segment with a volume in the top five percent.

At 393°K (Figure 10), it can be seen that the distribution of volume for neighbors of segments with large excess volume is very close to the distribution of volume for chain segments as a whole. A slight shift to higher volume is seen in the distribution for neighbors, but this is attributable to the process of Voronoi tessellation used. The shape of the distribution is essentially unchanged.

At 233°K (Figure 11), the difference in the distribution for neighbors of segments with large excess volume and the general segment volume distribution is more pronounced. The neighbor distribution is not only shifted upwards, but is seen to have a different shape. A sizable enlargement in the number of segments with larger than average volume over the general segment population is found. This suggests that the neighbors of chain segments with significantly larger than average volume are themselves significantly larger than the norm.

This implies that in the liquid state the segments with large excess volume are distributed more or less uniformly through the simulation volume. Below the glass transition, the tendency is more for the largest segments to be clustered with other segments of large volume. Thus the length scale of the inhomogeneity in the liquid is on the order of the size of the segments -- individual segments have different volumes associated with them, but larger regions look more alike. In the glass, the inhomogeneity extends beyond the segments and the picture of a glass becomes one of pockets of relatively low density (and presumably higher mobility) material embedded in a matrix of higher density (lower mobility)

polymer. The development of such inhomogeneity has been reported during simulations of the "amorphization" of crystals by irradiation [19].

One explanation of the glass transition which has been proposed on the basis of simulations of simple atomic liquids and glasses, is that the transition from glass to liquid occurs when local regions of material with excess volume ("liquid-like") increase in number and/or size until a percolation threshold is reached [20]. A continuous network of "liquid-like" material then exists and the macroscopic properties take on the characteristics of a liquid. A more detailed analysis than that described here is necessary to determine if this intuitively appealing concept can be applied to the polymer glass transition; it will be reported on in a later publication.

The study of the dynamics of the simulated polymer is not yet complete. However, the data of Figure 4 does indicate that some differences in the dynamics of the glass and liquid do exist. The generalized frequency spectrum in the region below 500 cm^{-1} is due mostly to backbone torsional modes. As can be seen, there are differences in this region between the spectra calculated for 233°K and 393°K. The lowest frequency peak, at 50-60 cm^{-1}, is enhanced in the high temperature spectra. Presumably, this is due to an increase in the amount of torsional motion taking place in this low frequency range.

The low frequency regime is amenable to probing through the use of inelastic neutron scattering. Studies of atactic poly(propylene) utilizing this technique are currently in progress. A future report will discuss the results of this and associated simulation work to identify the motions taking place, and how they affect the macroscopic properties of the polymer.

In summary, the development of a realistic molecular dynamics model for a simple vinyl polymer is reported. The model replicates the behavior of the actual polymer to an acceptable degree. Using the model, a study of how the structure and dynamics of the polymer differ in the liquid and glass states has been undertaken. Initial results obtained by examining the volume associated with the chain segments indicate that there is a significant broadening of the volume distribution above T_g. In addition, there is evidence that in the glassy state chain segments with much larger than average volume tend to segregate together, while in the liquid they are more uniformly dispersed. Very preliminary data on the dynamics of the system indicates that the model does show differences between simulations conducted at different temperatures. Work in progress with the molecular dynamic model will shed light on the finer details of the structural and dynamic differences between the liquid and glassy states. Additional work being carried out with a Monte Carlo model of atactic poly(propylene) will provide information on the kinematic pathways by which both one state can be reached from the other and the process of physical aging takes place.

Acknowledgement

This work was supported by the DARPA University Research Initiative through the Office of Naval Research under contract N00014-86-K-0768. The San Diego Supercomputer Center is acknowledged for a generous grant of time on a CRAY X-MP/48 on which some simulations were performed.

References

1. Theodorou, D. N. and Suter, U. W.; *Macromolecules*, **18**, 1467 (1985).

2. Kremer, K., Grest, G. S., and Carmesin, I.; *Physical Review Letters*, **61**, 566 (1988).

3. Clarke, J. H. R. and Brown, D.; *Molecular Simulation*, **3**, 27 (1989).

4. Boyd, R. H. and Pant, K.; *Amer. Chem Soc. Polymer Preprints*, **30**(2), 30 (1989).

5. Berman, D. and Weiner, J. H.; *J. Chemical Physics*, **83**, 1311 (1985).

6. Turnbull, D. and Cohen, M.H.; *J. Chemical Physics*, **34**, 120 (1961).

7. Cohen, M. H. and Grest, G. S.; *Physical Review B*, **20**, 1077 (1979).

8. Nosé, S.; *J. Chemical Physics*, **81**, 511 (1984).

9. Hoover, W. G.; *Physical Review A*, **31**, 1695 (1985),

10. Andersen, H. C.; *J. Chemical Physics*, **74**, 2384 (1980).

11. Nosé, S. and Klein, M. L.; *Molecular Physics*, **50**, 1055 (1983).

12. Lifson, S. and Warshel, A.; *J. Chemical Physics*, **49**, 5116 (1968).

13. Suter, U. W. and Flory, P. J.; *Macromolecules*, **8**, 765 (1975).

14. Voronoi, G. F.; *Z. Reine Angew. Math.*, **134**, 198 (1908).

15. Tanemura, M., Ogawa, T. and Ogita, N.; *J. Computational Physics*, **51**, 191 (1983).

16. Maeda, T.; "Structural Analysis of Atactic Polypropylene: A Study of the Glass Transition by X-ray Diffraction," *Master of Science Thesis*, Department of Materials Science and Engineering, University of Pennsylvania, August 1987.

17. Hummel, D. O.; "Atlas of Polymer and Plastic Analysis, Vol. 1," 2nd ed., (Hanser Verlag: Munich, 1979).

18. Kaufmann, H. S. and Falcetta, J. J.; "Introduction to Polymer Science and Technology," (Wiley: New York, 1977).

19. Hsieh, H. and Yip, S.; *Physical Review B*, **39**, 7476 (1989).

20. Deng, D., Argon, A. S., Yip, S.; *Phil. Trans. Royal Soc. London A*, in the press.

Table 1

Simulation Parameters

	HH	CH	RH	CC	CR	RR
ε_{ij} (kJ/mol)	0.31935	0.30176	0.37086	0.35197	0.44719	0.58112
σ_{ij} (Å)	2.3163	2.7617	2.9400	3.2072	3.3854	3.5636

	CH	CC	CR
C_{ij}^{bl} (kJ/Å^2)	3349.44	1674.72	1674.72
r_{ij}^{o} (Å)	1.0990	1.4712	1.5065

	HCH	a-HCC†	c-HCC†	HCR	a-CCC†	c-CCC†	RCC	RCR
C_{ijk}^{θ} (kJ/rad)	164.96	199.29	199.29	199.29	302.29	302.29	302.29	302.29
θ_{ijk}^{o} (radians)	1.9216	1.9190	1.8863	1.9246	1.8778	1.9380	1.9465	2.0559

C_{ijkl}^{ω} (kJ/mol)	2.800
W (kJ/mol-ps^2)	36992.8
Q (kJ/mol-ps^2)	7.39856

† a-HCC designates H-C-C valance angles where the central carbon is achiral.
c-HCC designates H-C-C valence angles where the central carbon is chiral.
a-CCC designates C-C-C valance angles where the central carbon is achiral.
c-CCC designates C-C-C valence angles where the central carbon is chiral.

Figure Captions

Figure 1a — The initial shape and size of the simulation cell is defined by the three vectors **a**, **b**, and **c**. The shape matrix **g** is formed using **a**, **b**, and **c** as its columns. The volume dilation variable L scales the components of **g** evenly. The real space positions of the atoms in the system are therefore defined by their position in a unit cube, $\mathbf{s}_i$, times **g** times L.

Figure 1b — The model polymer chain consists of carbon atoms (black), hydrogen atoms (white) and methyl groups (gray). Shown is a chain with degree of polymerization three and a terminal methyl group.

Figure 2 — The system is constructed by packing a chain such as that shown in a.) into the simulation cell through the use of periodic boundary conditions. 26 image chains are generated by translation of the chain along the **a**, **b**, and **c** axes of the cell by permutations of $[(-1,0,1), (-1,0,1), (-1,0,1)]$. This results in a cell, shown in b.) which contains portions of both the original chain and the image chains. Whenever a chain exits through one side of the cell, another chain enters from the opposite side.

Figure 3 — The low Q x-ray static structure factor obtained experimentally (●) and calculated from the radial distribution functions determined from simulation (—). The experimental results are taken from the work of Maeda [16] and represent the structure factor of atactic poly(propylene) at an indeterminate temperature near or above the glass transition. The calculated results were

obtained from simulations at 293°K using the method described by Theodorou [1].

Figure 4 The generalized frequency spectrum for atactic poly(propylene) at 233°K (—) and 393°K (—) was calculated as the Fourier transform of the velocity autocorrelation function, $c(t) = \langle \vec{r}(t) \bullet \vec{r}(0) \rangle / \langle \vec{r}(0) \bullet \vec{r}(0) \rangle$, where the average is taken over all atoms and $0 \leq t \leq 2.5$ ps. The tickmarks along the abscissa indicate the locations of infrared optical absorptions in an experimental spectrum from ref. 17.

Figure 5 The calculated (— ● —) specific volume versus temperature curve was obtained by allowing static polymer structures prepared by the method of Theodorou [1] at each temperature and the experimental specific volume (♦) to relax during molecular dynamics simulations to new mechanical equilibria following the removal of fixed bond lengths and angles and introduction of thermal motion. Each calculated point represents the average of three simulations while the error bars are the averaged standard deviations over 20 picoseconds. Regression lines through the three points above and below the experimental glass transition (253°K) intersect at 277°K while the slopes provide constant pressure thermal expansion coefficients that are close to the experimental values [18].

Figure 6 The distribution of volume associated with achiral CH_2 groups (—) and chiral CHR groups (—) at 233°K was calculated by carrying out a Voronoi tessellation of space based

on the recorded positions of the atoms in the system over the last 20 ps of each simulation. The Voronoi polyhedra for the three atoms in each group were joined together and the volume of the group computed. Each curve represents the average from tessellation of 250 "snapshots" for each of three simulations.

Figure 7 The distribution of volume associated with achiral CH_2 groups (—) and chiral CHR groups (—) at 393°K was calculated as described in Figure 6. The distributions at the higher temperature have a higher average value and are significantly broader than those at 233°K (Figure 6).

Figure 8 The average volume for the achiral (— o —) and chiral (— ● —) groups versus temperature shows the same behavior as is seen for the overall volume expansion (Figure 5). No evidence that one type of group contributes more to the expansion than the other can be seen.

Figure 9 The average standard deviation for the achiral (— o —) and chiral (— ● —) group volume distributions versus temperature shows an increase of 15-25% in the region of the apparent glass transition temperature for the polymer model.

Figure 10 The volume distribution of all segments at 393°K (—) is compared to the distribution for segments which are nearest neighbors to any segment which is in the top 5% of the achiral or chiral segment distributions (—) (Figure 7). The two curves

have similar shapes though the distributions for the neighbors of large segments is shifted upwards slightly.

Figure 11 The distribution of all segments at 233°K (—) is compared to that for those segments which are neighbors of the largest 5% of chiral or achiral segments (—) (Figure 6). The shape of the distribution for the neighbors of large segments is distorted considerably towards larger volumes, in addition to an upwards shift.

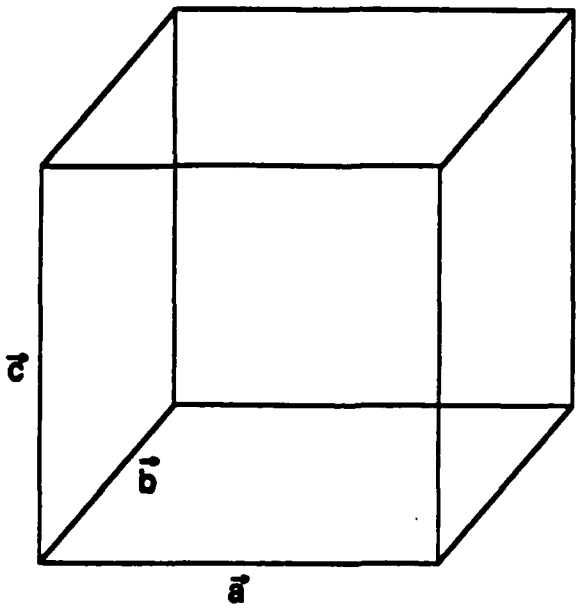

$$g = [\vec{a}\ \vec{b}\ \vec{c}]$$

Figure 1a

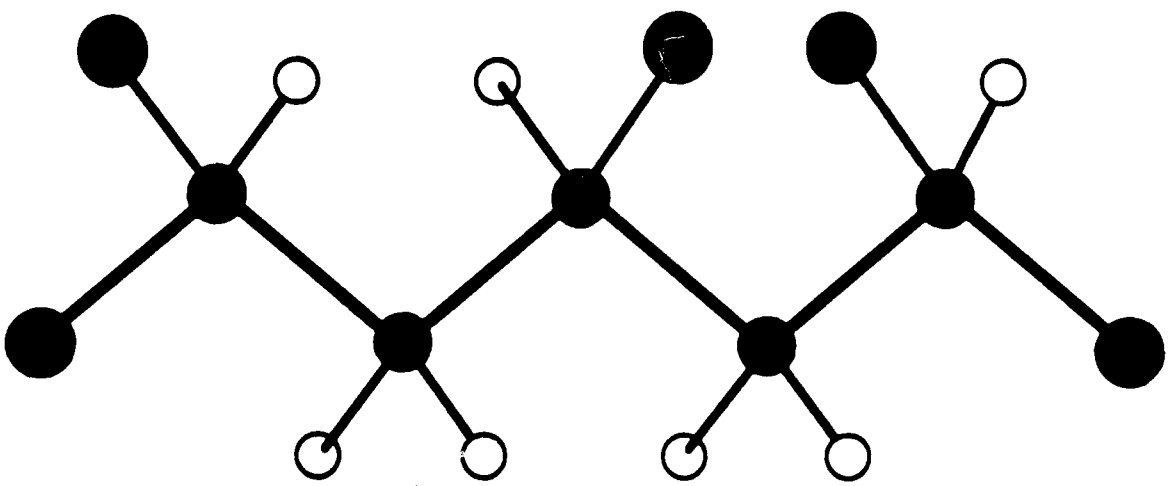

Figure 1b

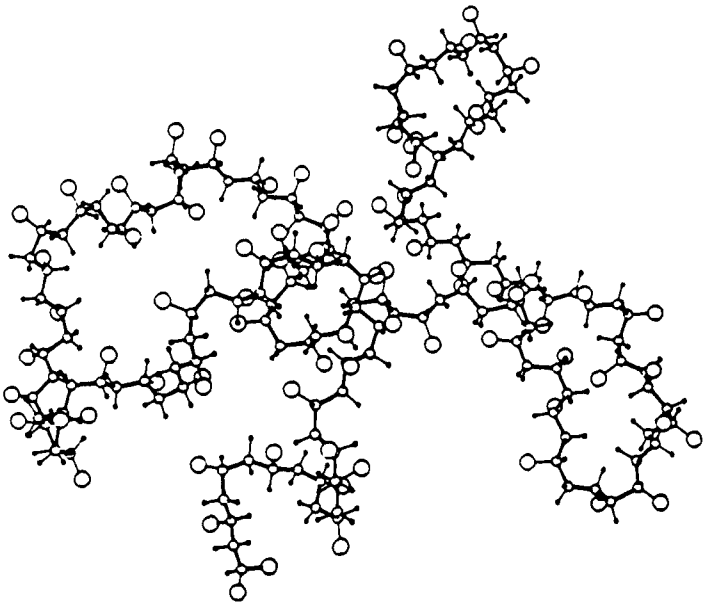

Figure 2a

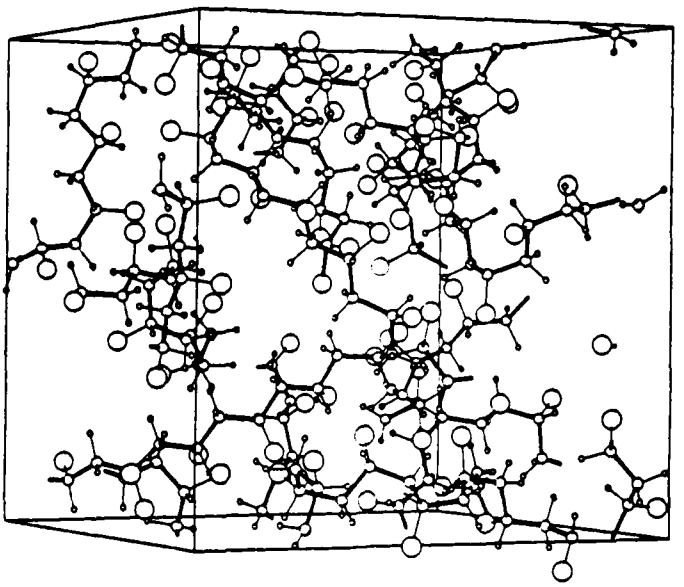

Figure 2b

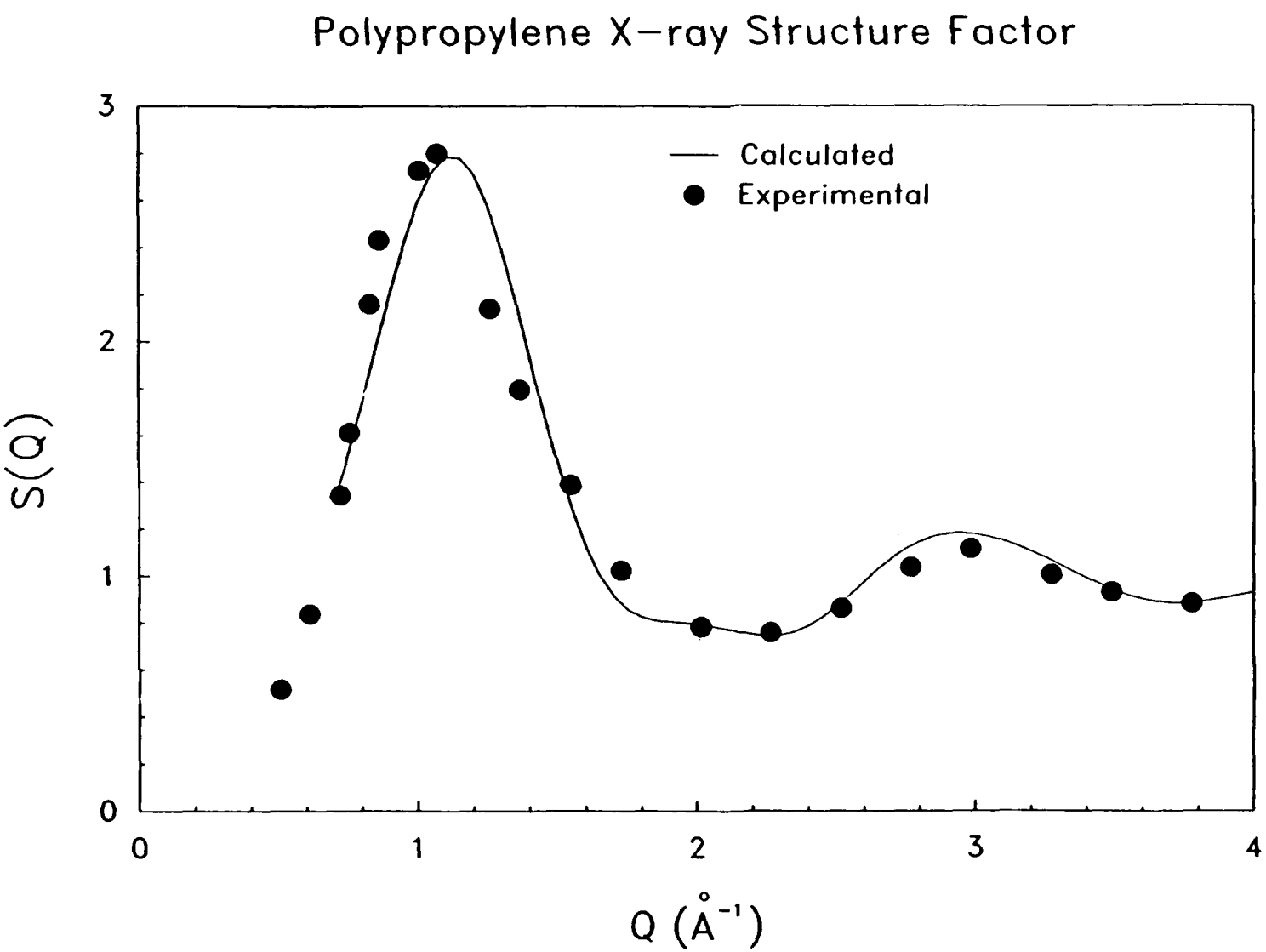
Polypropylene X-ray Structure Factor
Calculated
Experimental
S(Q)
Q (Å^{-1})
0
1
2
3
4

Figure 4

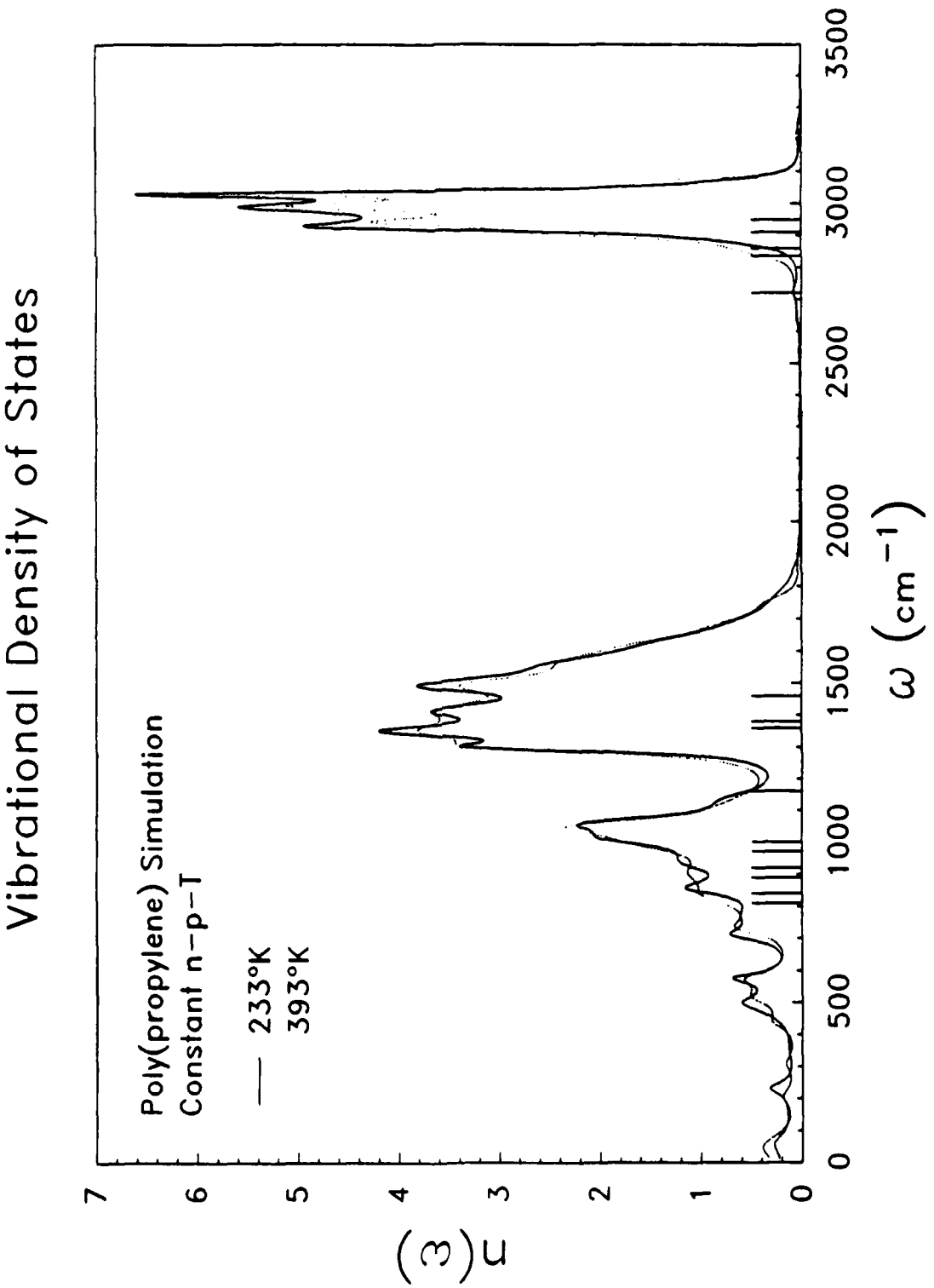
Vibrational Density of States
Poly(propylene) Simulation
Constant n-p-T
233°K
393°K
n(ω)
ω (cm⁻¹)
0
1
2
3
4
5
6
7
500
1000
1500
2000
2500
3000
3500

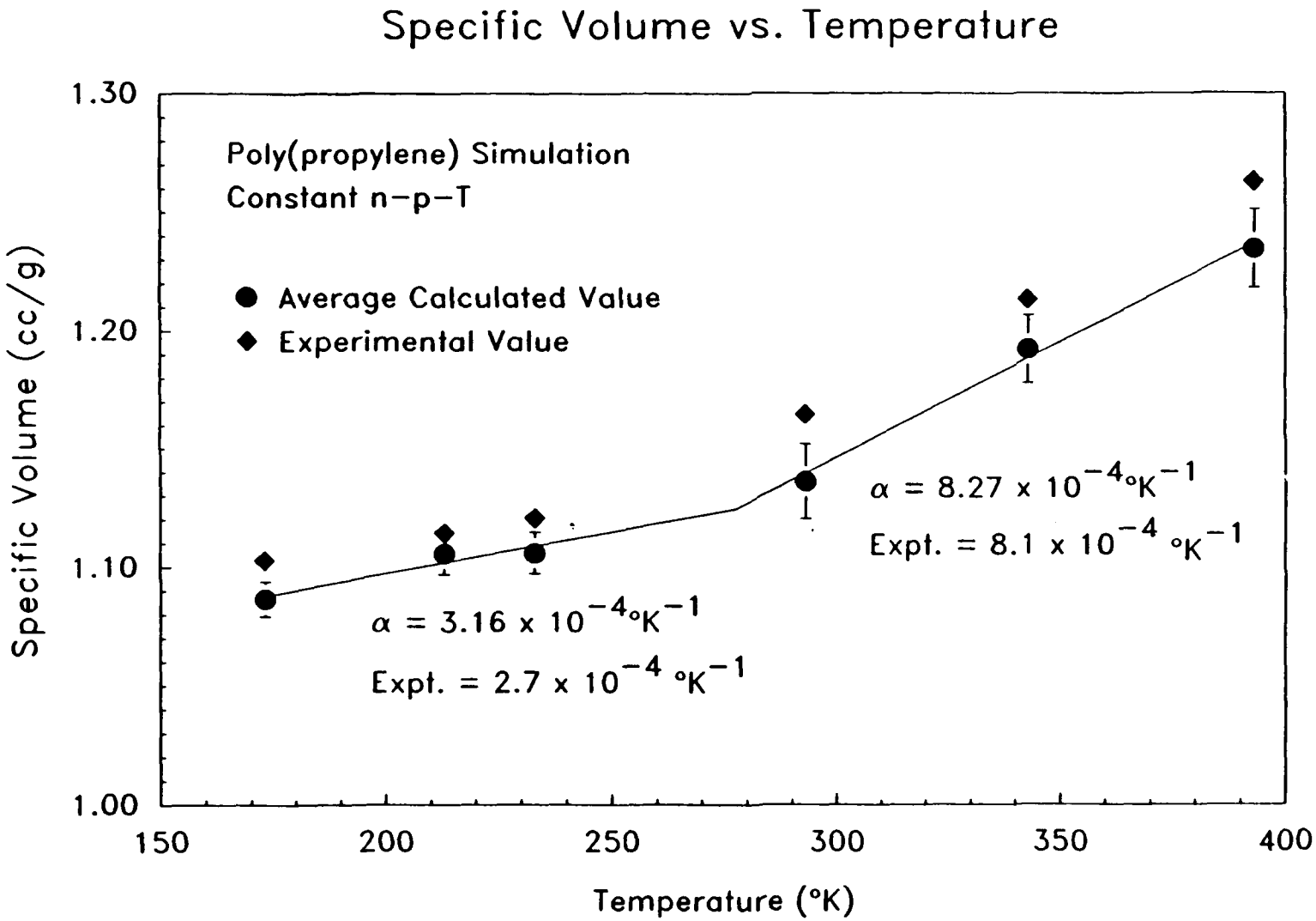
Specific Volume vs. Temperature
Poly(propylene) Simulation
Constant n−p−T
Average Calculated Value
Experimental Value
α = 3.16 x 10^−4 °K^−1
Expt. = 2.7 x 10^−4 °K^−1
α = 8.27 x 10^−4 °K^−1
Expt. = 8.1 x 10^−4 °K^−1
Specific Volume (cc/g)
1.30
1.20
1.10
1.00
150
200
250
300
350
400
Temperature (°K)

Figure 6

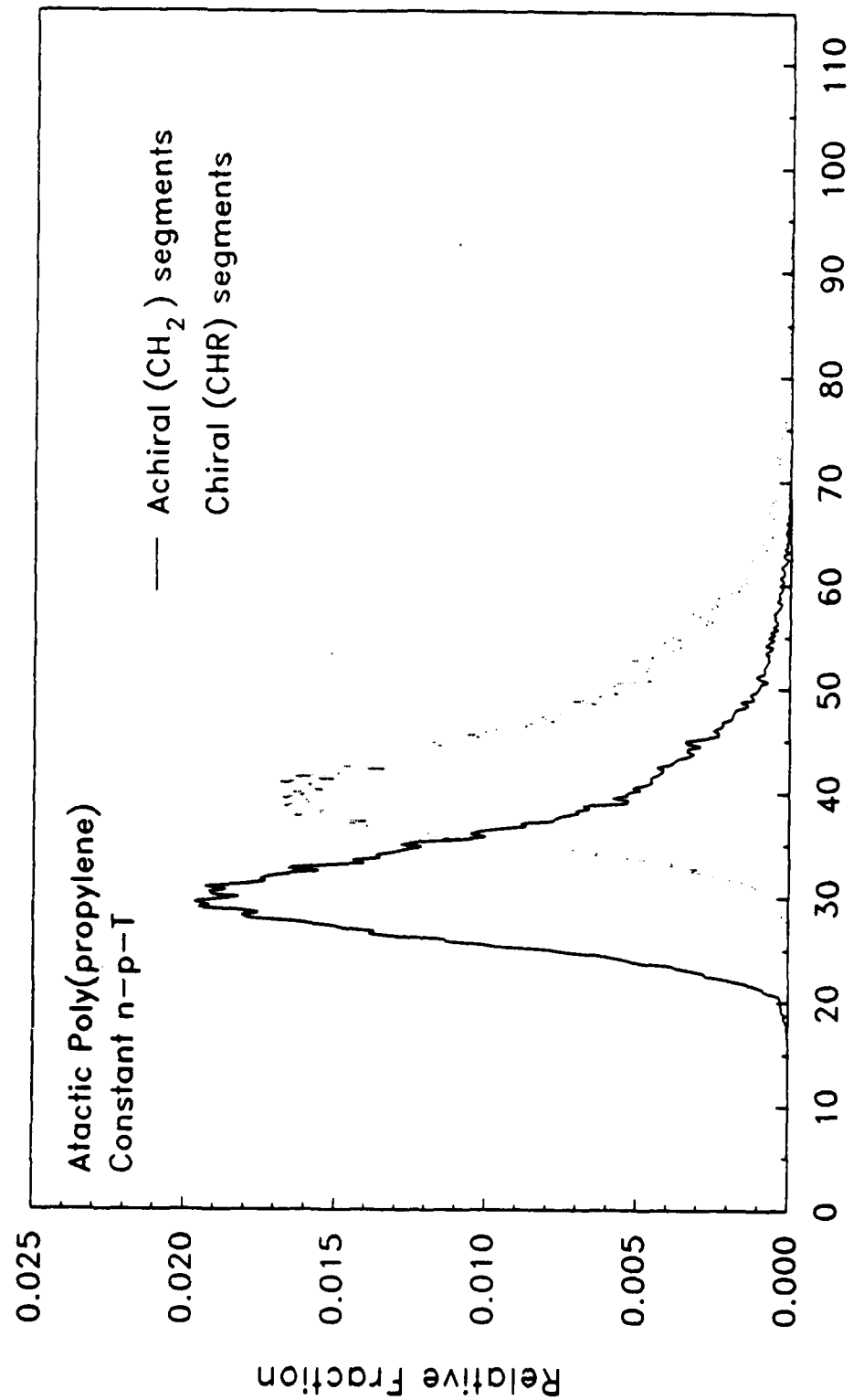
Segment Volume Distribution at 233°K
Atactic Poly(propylene)
Constant n-p-T
Achiral (CH_2) segments
Chiral (CHR) segments
Relative Fraction
0.025
0.020
0.015
0.010
0.005
0.000
0
10
20
30
40
50
60
70
80
90
100
110
Segment Volume ($Å^3$)

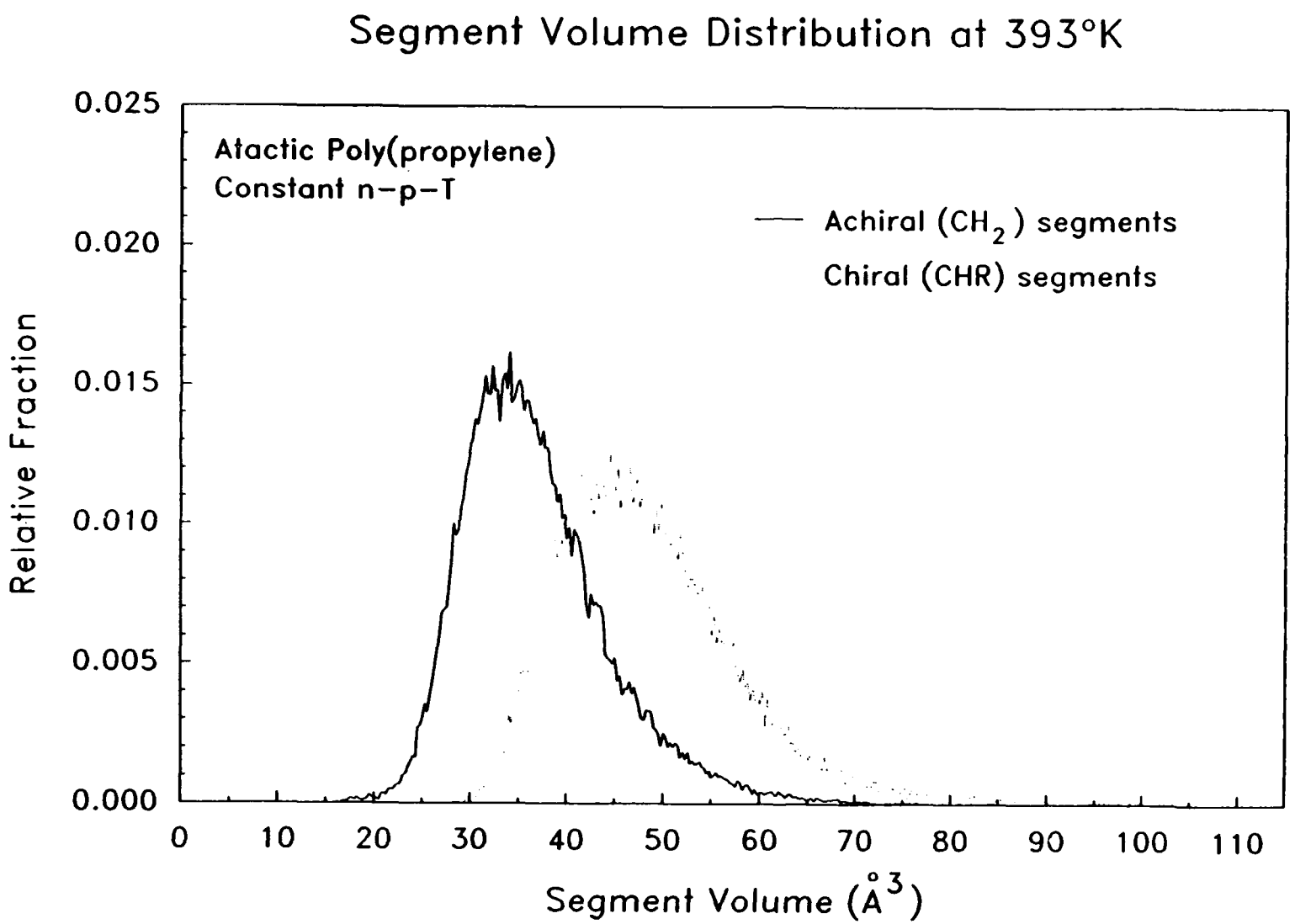
Segment Volume Distribution at 393°K
Atactic Poly(propylene)
Constant n-p-T
Achiral (CH_2) segments
Chiral (CHR) segments
Relative Fraction
0.025
0.020
0.015
0.010
0.005
0.000
0
10
20
30
40
50
60
70
80
90
100
110
Segment Volume ($Å^3$)

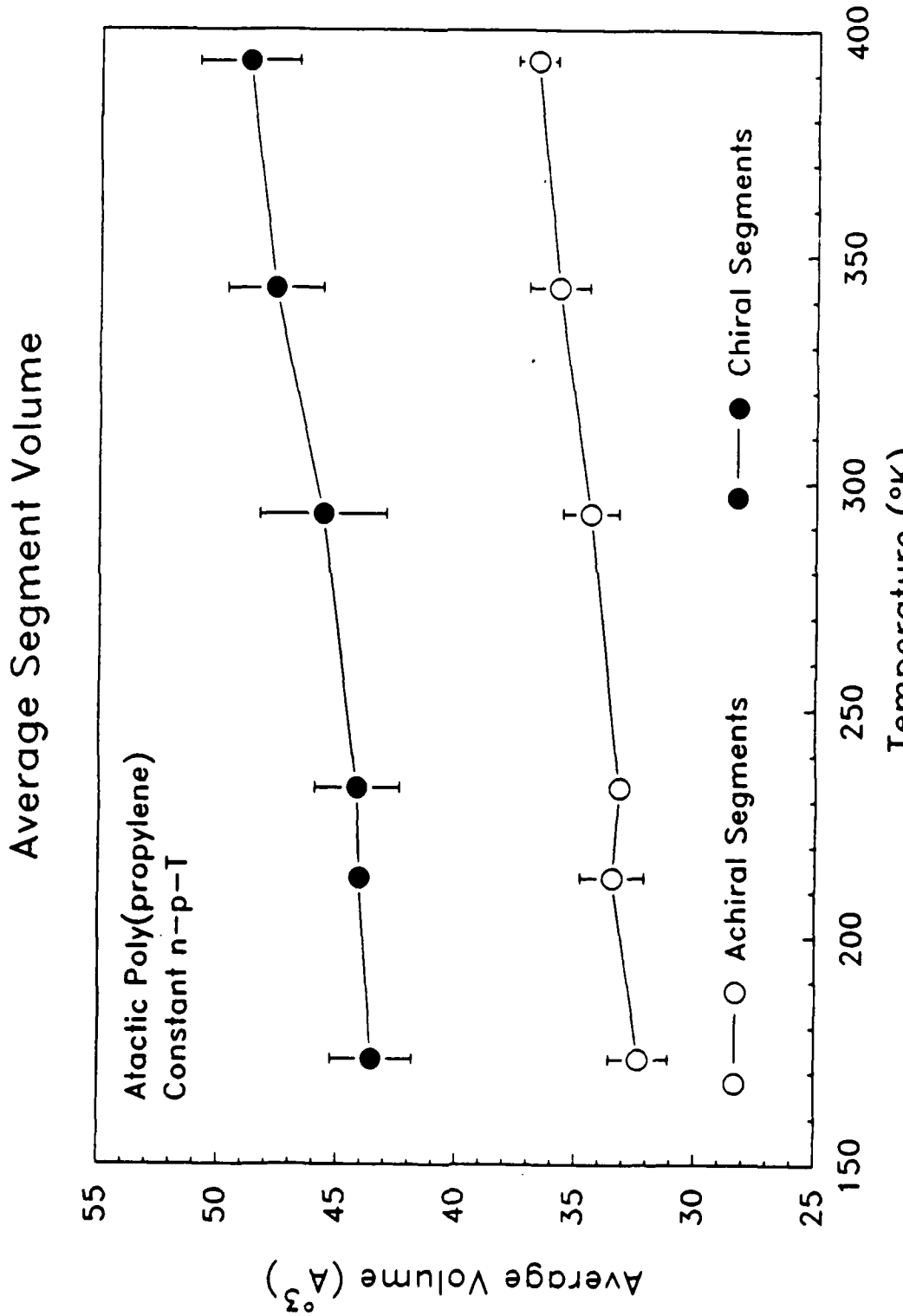
Average Segment Volume
Atactic Poly(propylene)
Constant n-p-T
Average Volume (A°3)
Temperature (°K)
Achiral Segments
Chiral Segments
55
50
45
40
35
30
25
150
200
250
300
350
400

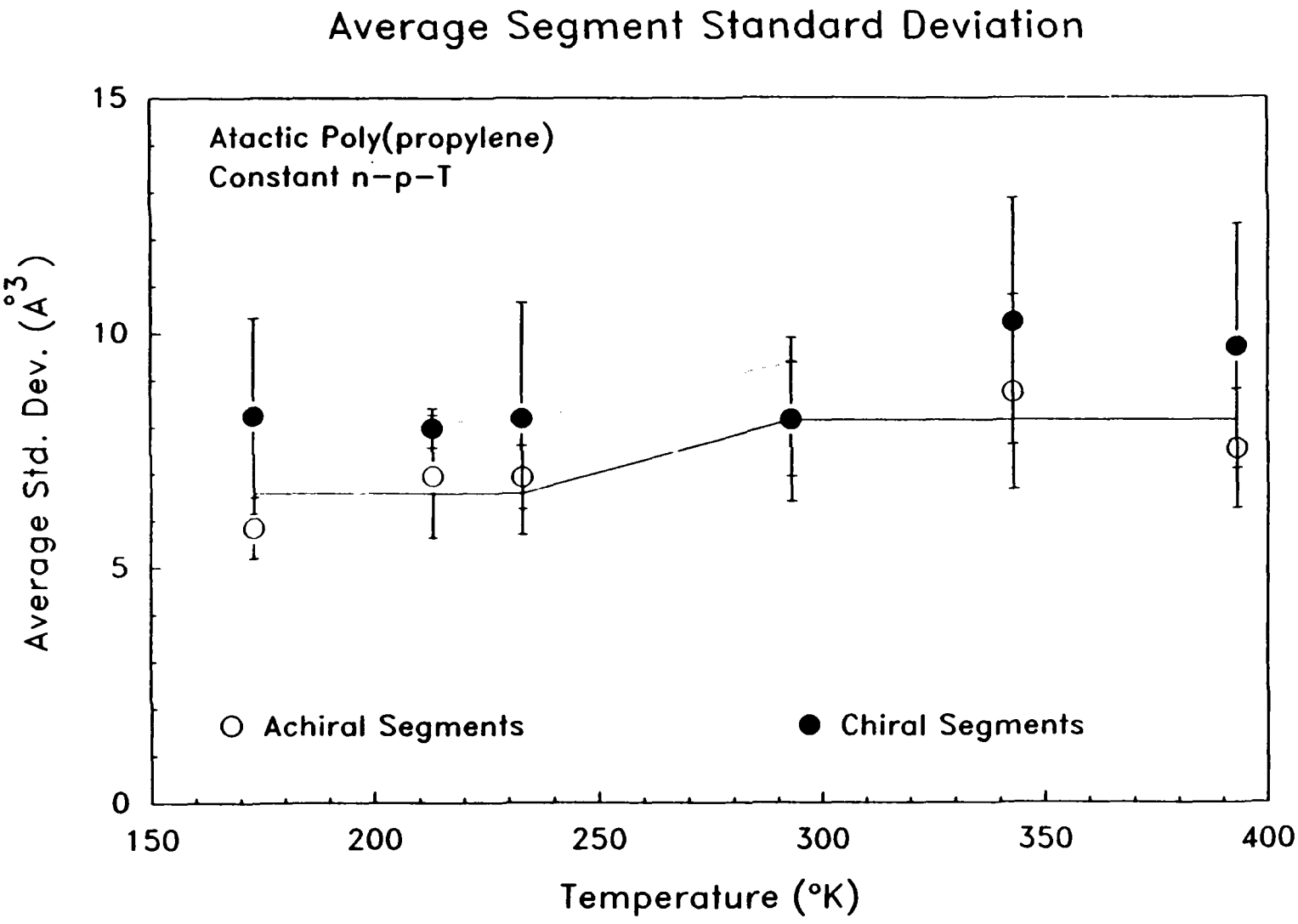
Average Segment Standard Deviation
Atactic Poly(propylene)
Constant n–p–T
Average Std. Dev. (A°3)
15
10
5
0
150
200
250
300
350
400
Temperature (°K)
○ Achiral Segments
● Chiral Segments

Figure 7.

Figure 10

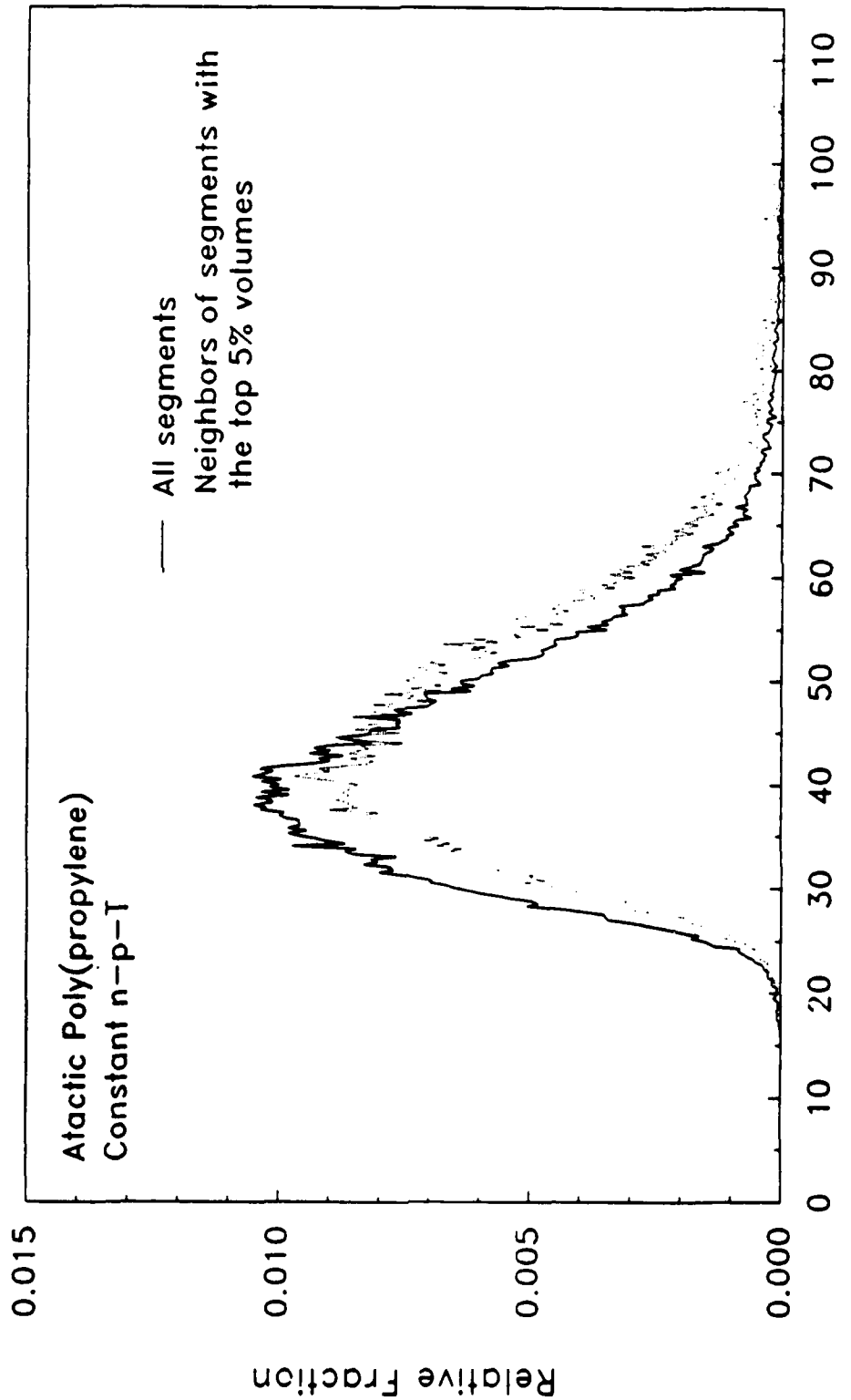
Segment Volume Distribution at 393°K
Atactic Poly(propylene)
Constant n-p-T
All segments
Neighbors of segments with the top 5% volumes
Relative Fraction
0.015
0.010
0.005
0.000
0
10
20
30
40
50
60
70
80
90
100
110
Segment Volume (Å3)

Figure 11

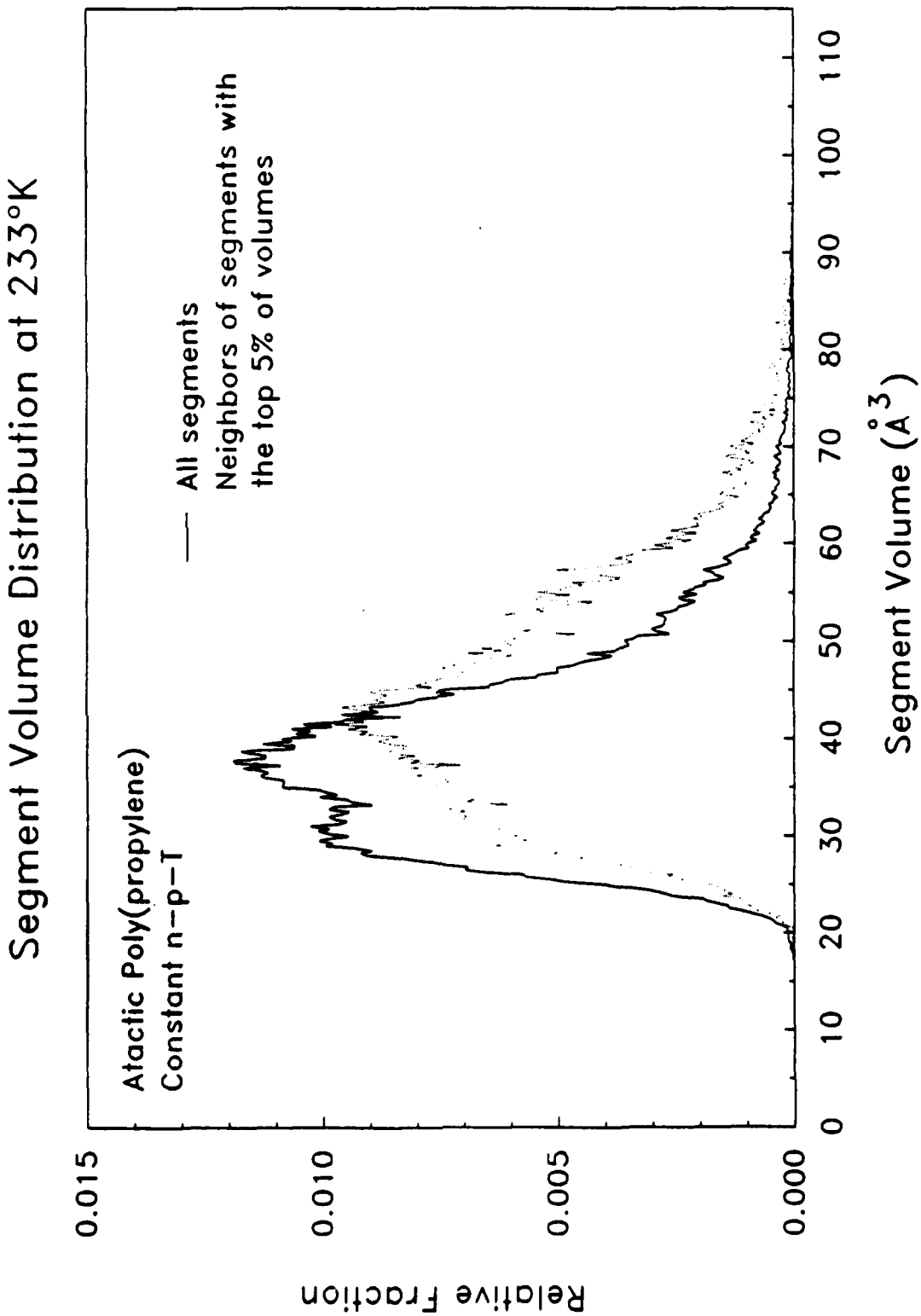
Segment Volume Distribution at 233°K
Atactic Poly(propylene)
Constant n-p-T
All segments
Neighbors of segments with
the top 5% of volumes
Relative Fraction
0.015
0.010
0.005
0.000
0
10
20
30
40
50
60
70
80
90
100
110
Segment Volume (Å3)